A&A 437, 9–22 (2005)
DOI: 10.1051/0004-6361:20041046

Astronomy & Astrophysics

Spiral density wave generation by vortices in Keplerian flows⋆

G. Bodo[1], G. Chagelishvili[3], G. Murante[1], A. Tevzadze[3], P. Rossi[1], and A. Ferrari[2]

[1] INAF Osservatorio Astronomico di Torino, Strada dell'Osservatorio 20, 10025 Pino Torinese, Italy
e-mail: bodo@to.astro.it
[2] Dipartimento di Fisica Generale dell'Università, via Pietro Giuria 1, 10125 Torino, Italy
[3] Center for Plasma Astrophysics, Abastumani Astrophysical Observatory, 2a Kazbegi Ave., Tbilisi 0160, Georgia

Received 7 April 2004 / Accepted 28 February 2005

Abstract. We perform a detailed analytical and numerical study of the dynamics of perturbations (vortex/aperiodic mode, Rossby and spiral-density waves) in 2D compressible disks with a Keplerian law of rotation. We draw attention to the process of spiral-density wave generation from vortices, discussing, in particular, the initial, most peculiar stages of wave emission. We show that the linear phenomenon of wave generation by vortices in smooth (without inflection points) shear flows found by using the so-called non-modal approach, is directly applicable to the present case. After an analytical non-modal description of the physics and characteristics of the spiral-density wave generation/propagation in the local shearing-sheet model, we follow the process of wave generation by small amplitude coherent circular vortex structures, by direct global numerical simulation, describing the main features of the generated waves.

Key words. accretion, accretion disks – waves – hydrodynamics

1. Introduction

The dynamics of vortices in astrophysical disks has recently received much interest both because vortices in protoplanetary disks can represent aggregation regions of solid particles for the eventual formation of planets (Barge & Sommeria 1995) and more generally for understanding accretion disk dynamics and the basic problem of angular momentum transport (Lovelace et al. 1999; Li et al. 2000). Several works have been devoted to the analysis of the possibility of forming and maintaining coherent vortex structures in the strongly sheared flow pertaining to a Keplerian disk, both in barotropic configurations, where the initial potential vorticity perturbation is conserved (Bracco et al. 1999; Godon & Livio 1999, 2000; Davis et al. 2000; Davis 2002) and in baroclinic situations where one can have vorticity generation (Klahr & Bodenheimer 2003; Klahr 2004). In the incompressible case it has been shown that coherent vortex structures can indeed form (under conservation of potential vorticity) and anticyclonic vortices can survive longer than cyclonic ones (Bracco et al. 1999) and give rise to the appearance of Rossby waves in the system (Davis et al. 2000). The effects of compressibility have not yet been fully analyzed and require rigorous study. Godon & Livio (1999) performed two-dimensional time-dependent numerical simulations of vortices in viscous compressible Keplerian disks. Vorticity waves are considered as one of the constituents of (anticyclonic) vortex dynamics, but without specification of the wave properties and any analysis of their genesis and dynamics (the subject of the study was the stability and lifetime of vortices). Davis (2002) performed fully compressible numerical simulations of the dynamics of a single vortical structure in a Keplerian disk flow and has reported the generation of outward-moving compressible waves by the coherent vortex (the generation was attributed to nonlinear processes) pointing out the potential importance of this phenomenon for vortex dynamics. Johansen et al. (2004) considered the dynamics of nonlinear vortices by numerical 3D simulations in the local shearing sheet approximation, also observing indications of wave generation. Klahr & Bodenheimer (2003), performing 2D and 3D hydrodynamical simulations of protoplanetary disks, found that a radial entropy gradient can generate Rossby waves which eventually break into vortices. Klahr (2004), by a linear stability analysis similar to the one presented in this paper, in fact showed that a radial entropy gradient leads to continuous generation of potential vorticity and to a transient swing-like amplification of the vortical/aperiodic mode, without the subsequent decay observed in the linear barotropic configuration.

The aim of this paper is to investigate the linear dynamics of initially-imposed vortical perturbations in 2D compressible Keplerian disks to understand the phenomena of spiral-density and Rossby wave generation and to study the initial, most peculiar stages of wave emission/propagation. In this repect, we want to stress that the origins of spiral-density and Rossby waves are absolutely different.

We base our understanding of spiral-density wave generation on the papers by Chagelishvili et al. (1997, 2000), where

⋆ Appendix A is only available in electronic form at
http://www.edpsciences.org

a completely linear phenomenon of acoustic wave generation by vortex mode perturbation in smooth shear flows was for the first time discussed. It was also shown that the generated acoustic waves are emitted as two symmetric packages in opposite directions from the parent coherent vortex perturbation. This wave generation phenomenon is directly applicable to the generation of spiral-density waves by vortices in disk flows (Sect. 3). The Rossby wave appearance from the vortex mode perturbations, on the contrary, is not connected to any generation process. The essence of the Rossby wave formation lies in the "breaking of degeneracy" of vortex mode perturbations (Sect. 4).

Recently, much progress has been made by the hydrodynamic community in the analysis of the linear dynamics of smooth shear flows by recognising that the traditional normal mode approach does not represent the best tool for its study because of the non-normality of the linear operators in the flows (cf. Reddy et al. 1993; Henningson & Reddy 1994; Gustavsson 1991; Farrell & Ioannou 1993; Craik & Criminale 1986). This means that the corresponding eigenfunctions are not orthogonal and strongly interfere. The knowledge drawn from the analysis of separate eigenfunctions and eigenvalues is far from complete. A correct and full description of the shear flow phenomena needs knowledge of the interference processes which cannot be easily taken into account in the framework of modal analysis. These circumstances led to the development of the so-called non-modal approach that could reveal several unexpected phenomena, which were overlooked by the normal mode analysis. The non-modal analysis is a modification of the initial value problem. It involves the change of independent variables from the laboratory to a moving frame and the study of the temporal evolution of spatial Fourier harmonics (SFH) of perturbations without any spectral expansion in time. The resulting linear dynamics is much richer than that expected from the stability predictions of the modal approach and these linear processes may also play a fundamental role in the full dynamics of smooth shear flows. For example, it has been shown that vortical perturbations can have a phase of transient amplification, which is at the base of the so-called "bypass" concept of the onset of turbulence in planar Couette flows (Baggett et al. 1995; Gebhardt & Grossman 1994; Farrell & Ioannou 1993; Henningson & Ready 1994; Grossmann 2000; Chagelishvili et al. 2002; Chapman 2002). Another phenomenon of interest here is the generation of waves by a vortex/aperiodic mode of perturbations, which has been discussed for the first time, as we saw above, by Chagelishvili et al. (1997) and analyzed by Chagelishvili et al. (2000) and Farrell & Ioannou (2000) in the simplest planar configuration. In this paper we extend the non-modal analysis of this process to the case of 2D Keplerian disk flow (that is a natural example of smooth shear flows) in the shearing sheet approximation, giving the theoretical basis to understand the results of simulations like those presented by Davis (2002). We also perform numerical simulations of the vortex dynamics in Keplerian disks: we consider a small amplitude (to include only linear processes), coherent circular vortex and focus on wave generation and emission, on the properties of density and vorticity fields and on the description of the wave propagation trajectories. Physical model and equations are presented in Sect. 2. The non-modal analysis of spiral-density wave generation/emission by vortex mode perturbation is presented in Sect. 3. The appearance of the Rossby wave from vortex mode perturbation is outlined in Sect. 4. Numerical simulations of wave emergence from a coherent circular vortex perturbation is presented in Sect. 5 and in the last section we summarize our results. In the Appendix we describe the method for the selection of initial values of pure vortex mode perturbations for our numerical study.

2. Physical model and equations

In cylindrical coordinates, the basic equations will read as follows:

$$\frac{\partial \rho}{\partial t} + \frac{1}{r}\frac{\partial}{\partial r}(r\rho V_r) + \frac{1}{r}\frac{\partial}{\partial \phi}(\rho V_\phi) = 0, \tag{1}$$

$$\frac{\partial V_r}{\partial t} + (\mathbf{V}\nabla)V_r - \frac{V_\phi^2}{r} = -\frac{1}{\rho}\frac{\partial P}{\partial r} - \frac{\partial \Phi}{\partial r}, \tag{2}$$

$$\frac{\partial V_\phi}{\partial t} + (\mathbf{V}\nabla)V_\phi + \frac{V_r V_\phi}{r} = -\frac{1}{\rho r}\frac{\partial P}{\partial \phi}, \tag{3}$$

$$\left(\frac{\partial}{\partial t} + (\mathbf{V}\nabla)\right)P = \gamma\frac{P}{\rho}\left(\frac{\partial}{\partial t} + (\mathbf{V}\nabla)\right)\rho, \tag{4}$$

where

$$(\mathbf{V}\nabla) \equiv V_r\frac{\partial}{\partial r} + \frac{V_\phi}{r}\frac{\partial}{\partial \phi}. \tag{5}$$

We consider a two dimensional (2D) inviscid, differentially rotating flow. The flow has axial symmetry and a rotation axis parallel to the z axis: $\boldsymbol{V}_0 = (0, V_{0\phi}, 0)$, with $V_{0\phi} = r\Omega(\boldsymbol{r})$. In this flow configuration the basic force balance is described by:

$$r\Omega^2(r) = \frac{1}{\rho_0}\frac{\partial P_0}{\partial r} + \frac{\partial \Phi(\boldsymbol{r})}{\partial r}, \tag{6}$$

We choose a distribution of angular velocity that follows the Keplerian law

$$\Omega^2(\boldsymbol{r}) \propto \frac{1}{r^3}, \tag{7}$$

and a gravitational potential that balances the centrifugal term

$$\Phi(\boldsymbol{r}) \propto -\frac{1}{r}, \tag{8}$$

the pressure is then constant and equal to P_0.

Our 2D model of a Keplerian disk retains the dynamical effects of differential rotation, while discarding geometrical and thermodynamic (P_0, ρ_0 = const.) complications. The sound speed is defined by:

$$c_s^2 = \frac{\gamma P_0}{\rho_0} = \text{const.} \tag{9}$$

with the specific heat ratio $\gamma = 5/3$. Even though our flow is two-dimensional and has no z dependence, it is useful for the discussion to introduce the parameter

$$H = c_s/\Omega, \tag{10}$$

that represents the equivalent thickness of a thin disk model.

In a Keplerian disk the basic flow vorticity is (cf. Tagger 2001):

$$W = \frac{1}{2\Omega}\left[4\Omega^2 + 2\Omega\left(r\frac{\partial\Omega}{\partial r}\right)\right] = \frac{\Omega}{2}. \tag{11}$$

Thus, the mean vorticity gradient across the disk is nonzero and should not a priori be neglected.

3. Linear dynamics of vortex mode – generation of spiral-density waves

Here we study the linear dynamics of 2D small-scale perturbations (i.e. with characteristic scales in radial and azimuthal directions much less than the radial characteristic scale of the background/disk flow) in the shearing sheet approximation (e.g., Goldreich & Lynden-Bell 1965; Goldreich & Tremaine 1978; Nakagawa & Sekiya 1992). In this case the dynamical equations are written in the local co-moving Cartesian coordinate system:

$$x \equiv r - r_0; \quad y \equiv r_0(\phi - \Omega_0 t); \quad \frac{x}{r_0}, \frac{y}{r_0} \ll 1, \tag{12}$$

where (r, ϕ) are standard cylindrical co-ordinates and Ω_0 is the local rotation angular velocity at $r = r_0$:

$$\Omega(r) = \Omega_0 + \frac{\partial\Omega}{\partial r}(r - r_0) \equiv \Omega_0 + 2A\frac{x}{r_0}, \tag{13}$$

where

$$A \equiv \frac{1}{2}\left[r\frac{\partial\Omega}{\partial r}\right]_{r=r_0} \tag{14}$$

is the standard Oort constant which describes the mean velocity shear parameter in the local frame. In the case of a Keplerian rotation law:

$$A = -\frac{3}{4}\Omega_0 < 0. \tag{15}$$

The main assumption of the shearing sheet approximation is the neglect of the basic flow vorticity gradient; the only gradient being considered is differential rotation.

Introducing linear perturbations

$$\boldsymbol{V} = \boldsymbol{V}_0 + \boldsymbol{v}', \quad P = P_0 + p', \quad \rho = \rho_0 + \rho', \tag{16}$$

we derive, from system (1)−(4), the equations governing the linear dynamics of perturbations in the local Cartesian frame:

$$\left(\frac{\partial}{\partial t} + 2Ax\frac{\partial}{\partial y}\right)v_x' - 2\Omega_0 v_y' + \frac{1}{\rho_0}\frac{\partial p'}{\partial x} = 0, \tag{17}$$

$$\left(\frac{\partial}{\partial t} + 2Ax\frac{\partial}{\partial y}\right)v_y' + 2(\Omega_0 + A)v_x' + \frac{1}{\rho_0}\frac{\partial p'}{\partial y} = 0, \tag{18}$$

$$\left(\frac{\partial}{\partial t} + 2Ax\frac{\partial}{\partial y}\right)\rho' + \rho_0\left(\frac{\partial v_x'}{\partial x} + \frac{\partial v_y'}{\partial y}\right) = 0, \tag{19}$$

$$\left(\frac{\partial}{\partial t} + 2Ax\frac{\partial}{\partial y}\right)p' + c_s^2\left(\frac{\partial}{\partial t} + 2Ax\frac{\partial}{\partial y}\right)\rho' = 0. \tag{20}$$

Hence, following the standard method of non-modal analysis (cf. Goldreich & Lynden-Bell 1965; Goldreich & Tremaine 1978), we introduce the spatial Fourier harmonics (SFH) of perturbations with time-dependent phases:

$$\begin{Bmatrix} v_x'(\boldsymbol{r}, t) \\ v_y'(\boldsymbol{r}, t) \\ p'(\boldsymbol{r}, t) \\ \rho'(\boldsymbol{r}, t) \end{Bmatrix} = \begin{Bmatrix} v_x(k_x(t), k_y, t) \\ v_y(k_x(t), k_y, t) \\ p(k_x(t), k_y, t) \\ \varrho(k_x(t), k_y, t) \end{Bmatrix} \exp(\mathrm{i}k_x(t)x + \mathrm{i}k_y y) \tag{21}$$

$$k_x(t) = k_x(0) - 2Ak_y t = k_x(0) + \frac{3}{2}\Omega_0 k_y t. \tag{22}$$

The streamwise/azimuthal wavenumber remains constant and the streamcross/radial wavenumber changes at a constant rate; in the linear approximation SFH "drifts" in the $\boldsymbol{k}$-plane (wavenumber plane). The effect of this change is that lines of constant phase (wave crests) are rotated by the basic flow.

Substitution of Eqs. (21), (22) into Eqs. (17)−(20) yields the system of ordinary differential equations that governs the linear dynamics of SFH of perturbations in the described flow:

$$\frac{\mathrm{d}v_x(t)}{\mathrm{d}t} = 2\Omega_0 v_y(t) - \mathrm{i}k_x(t)\frac{p(t)}{\rho_0}, \tag{23}$$

$$\frac{\mathrm{d}v_y(t)}{\mathrm{d}t} = -2(\Omega_0 + A)v_x(t) - \mathrm{i}k_y\frac{p(t)}{\rho_0}, \tag{24}$$

$$\frac{\mathrm{d}\varrho(t)}{\mathrm{d}t} + \mathrm{i}\rho_0\left[k_x(t)v_x(t) + k_y v_y(t)\right] = 0, \tag{25}$$

$$p(t) = c_s^2\varrho(t). \tag{26}$$

Introducing $D(t) \equiv \mathrm{i}\varrho(t)/\rho_0$, Eqs. (23)−(26) become:

$$\frac{\mathrm{d}v_x(t)}{\mathrm{d}t} = 2\Omega_0 v_y(t) - k_x(t)c_s^2 D(t), \tag{27}$$

$$\frac{\mathrm{d}v_y(t)}{\mathrm{d}t} = -2(\Omega_0 + A)v_x(t) - k_y c_s^2 D(t), \tag{28}$$

$$\frac{\mathrm{d}D(t)}{\mathrm{d}t} = k_x(t)v_x(t) + k_y v_y(t). \tag{29}$$

Klahr (2004) obtained a similar system of equations for a configuration with a radial entropy gradient in the basic state, in that case he gets a fourth order system, while in our case, as we will see, the system can be reduced to second order.

The latter system is characterized by the important time invariant:

$$k_x(t)v_y(t) - k_y v_x(t) + 2(\Omega_0 + A)D(t) \equiv \mathit{I} \tag{30}$$

that follows (for SFH of perturbations) from the conservation of potential vorticity. This time invariant, in turn, indicates the existence of the vortex/aperiodic mode in the perturbation spectrum whose dynamics represent the main interest of this section. A radial entropy gradient would introduce a source term for potential vorticity (Klahr 2004) and the quantity above would no longer be invariant.

We can define the spectral density of the total energy in the $\boldsymbol{k}$-plane as:

$$E_{\boldsymbol{k}}(t) \equiv \frac{\rho_0}{2}\left(v_x^2 + v_y^2\right) + \frac{\rho_0 c_s^2}{2}D^2, \tag{31}$$

where the two terms correspond to the kinetic and potential energies of SFH.

The numerical study of SFH dynamics is governed by Eqs. (27)−(30). However, for the fundamental comprehension of the physical nature of the perturbations and their linear dynamics in the flow, we rewrite them in another form: from Eqs. (27)−(30) one can get the following second order *inhomogeneous* differential equation for $v_y(t)$:

$$\frac{\mathrm{d}^2 v_y(t)}{\mathrm{d}t^2} + \omega_{\mathrm{SD}}^2(t) v_y(t) = k_x(t) c_{\mathrm{s}}^2 \mathit{I}, \tag{32}$$

and the equations expressing $v_x(t)$ and $D(t)$ as functions of $v_y(t)$ and its time derivative:

$$v_x(t) = \frac{1}{4(\Omega_0 + A)^2 + k_y^2 c_{\mathrm{s}}^2} \times \left[k_x(t) k_y c_{\mathrm{s}}^2 v_y(t) - 2(\Omega_0 + A) \frac{\mathrm{d}v_y(t)}{\mathrm{d}t} - k_y c_{\mathrm{s}}^2 \mathit{I} \right], \tag{33}$$

$$D(t) = \frac{1}{2(\Omega_0 + A)} \left[k_x(t) v_y(t) - k_y v_x(t) - \mathit{I} \right], \tag{34}$$

where

$$\omega_{\mathrm{SD}}^2(t) \equiv 4\Omega_0(\Omega_0 + A) + k^2(t) c_{\mathrm{s}}^2 = \Omega_0^2 + k^2(t) c_{\mathrm{s}}^2, \tag{35}$$

and $k^2(t) \equiv k_x^2(t) + k_y^2$.

Equation (32) describes two different modes of perturbations:

(a) Spiral-density wave mode ($v_y^{(\mathrm{w})}$), that is described by the general solution of the corresponding homogeneous equation. Notice that the frequency of the wave $\omega(t)$ is time-dependent.

(b) Vortex mode ($v_y^{(\mathrm{v})}$), that is aperiodic, originates from the equation inhomogeneity ($k_x(t) c_{\mathrm{s}}^2 \mathit{I}$) and is associated with the particular solution of the inhomogeneous equation. The amplitude of the vortex mode is proportional to I and goes to zero when $\mathit{I} = 0$. The existence of the vortex/aperiodic mode, as discussed in more detail in Sect. 4, is the result of the main assumption of the shearing sheet approximation, i.e. the neglect of the basic flow vorticity gradient. Also, the vortex mode acquires nonzero divergence and nonzero density perturbation ($D^{(\mathrm{v})} \neq 0$, where $D^{(\mathrm{v})}$ is the density perturbation of the vortex mode as defined below).

Thus, we can decompose any perturbation as the sum of the wave and vortex mode perturbations:

$$v_x = v_x^{(\mathrm{w})} + v_x^{(\mathrm{v})}; \quad v_y = v_y^{(\mathrm{w})} + v_y^{(\mathrm{v})}; \quad D = D^{(\mathrm{w})} + D^{(\mathrm{v})}. \tag{36}$$

Clearly, the character of the dynamics depends on which mode of perturbation is imposed initially in Eqs. (27)−(29): pure waves (without mixture of aperiodic vortices), pure aperiodic vortices (without mixture of waves) or a mixture of the two.

Here we present a numerical and qualitative study of the linear dynamics of an initially excited SFH of vortex mode perturbation. The dynamics is defined by the value of the parameter:

$$R(t) \equiv \frac{2|A|}{\sqrt{4\Omega_0(\Omega_0 + A) + [k_x^2(t) + k_y^2] c_{\mathrm{s}}^2}} = \frac{3}{2\sqrt{1 + [k_x^2(t) + k_y^2] H^2}}, \tag{37}$$

where H is the equivalent thickness of a thin disk model defined in Eq. (10). $R(t)$ is a time-dependent parameter and consequently, the character of the dynamics is also time-dependent. The final result of the dynamics is defined by the maximum value of $R(t)$ (achieved at $t = t^*$, when $k_x(t^*) = 0$):

$$R_{\max} = \frac{3}{2\sqrt{1 + k_y^2 H^2}} \equiv \frac{3}{2\sqrt{1 + (mH/R)^2}}, \tag{38}$$

where m is the azimuthal wave-number of perturbation SFH.

We carried out numerical integration of Eqs. (27)−(29) for an initially imposed leading vortex mode SFH ($k_x(0)/k_y < 0$), without mixture of waves. Initial vortex SFH perturbations are defined by the equations presented in the Appendix. The calculations show a fundamental difference in the dynamics of vortices at low and moderate $R_{\max}$.

At $R_{\max} \ll 1$ all dynamics occurs at small $R(t)$, at low shear rates compressibility is negligible and only one phenomenon occurs, i.e. transient growth of SFH of aperiodic vortices. The leading SFH gains energy from the mean flow and increases its amplitude; when the SFH becomes trailing, it gives back the energy to the flow and decreases its amplitude. It is obvious that the transient growth of vortex perturbations exists in the spectrally/asymptotically stable flow system (the rotation curve derived from Kepler's law is extremely stable based on the Rayleigh criterion). The transient growth of two dimensional vortical/aperiodic perturbations in an incompressible Keplerian flow was found by Lominadze et al. (1988). Later on, the existence of transient growth was confirmed by Fridman (1989) and Ioannou & Kakouris (2001). The importance of transient growth for the onset of hydrodynamic turbulence in Keplerian disks is discussed by Chagelishvili et al. (2003) and Tevzadze et al. (2003).

At moderate/large $R_{\max}$, the dynamics are richer: our calculations show the appearance of a conversion of vortices to spiral-density waves at moderate shear rates. In Figs. 1−2 we present the results of calculations at $R_{\max} = 1.06;\ 1.34$ (respectively $m = R/H$ and $m = 0.5R/H$ in terms of the azimuthal wavenumber) . We can start to notice the conversion at about $R_{\max} \simeq 1$ (i.e., at about $k_y H \simeq 0.7$), but the overall behavior is still dominated by the vortex transient growth, as is evident from the lower right panel in Fig. 1 that shows the SFH energy growth and decrease. The process already becomes dominant in the SFH dynamics at $R_{\max} > 1.2$ (i.e., at about $k_y H < 0.5$).

In Fig. 2 we present the evolution of non-dimensional perturbed quantities ($v_x/c_{\mathrm{s}}, v_y/c_{\mathrm{s}}, D$) and of the normalized energy ($E_{\boldsymbol{k}}/E_{\boldsymbol{k}}(0)$) of a SFH, for the case with $R_{\max} = 1.34$. In this case, at the beginning $R(t) \ll 1$ (as $k_x(0)/k_y = -15$, i.e., $(k_x(0)/k_y)^2 \gg 1$), and the initial stage of the evolution is incompressible. Evolving in the shear flow, the vortex SFH gains energy from the mean flow and amplifies, while retaining its aperiodic nature. $R(t)$ increases, becomes moderate and compressibility comes into effect. As a result, we observe the appearance of an oscillating part of SFH, i.e. we observe the appearance of spiral-density waves. Thus, the linear dynamics of a vortex mode perturbation is followed by the generation of a spiral-density wave. When $R(t)$ is moderate, the time scales of

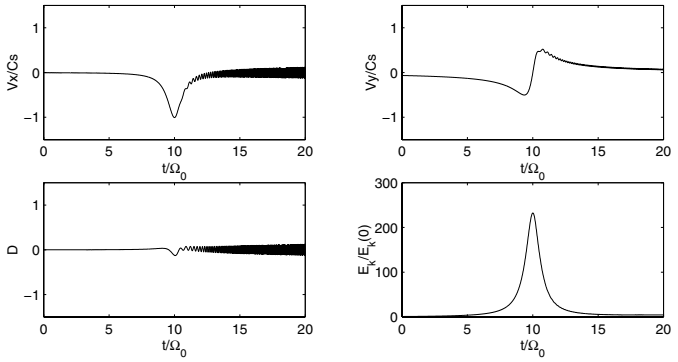

Fig. 1. The evolution of SFH normalized velocity and density perturbations (v_x/c_s, v_y/c_s and $D \equiv i\varrho/\rho_0$) and its normalized energy ($E_{\boldsymbol{k}}(t)/E_{\boldsymbol{k}}(0)$) at $R_{\max} = 1.06$ ($m = R/H$ in terms of the azimuthal wavenumber). In the dynamics of the initially imposed vortex SFH (with $k_x(0)/k_y = -15$, $k_y = 1$) transient growth is dominant, but the wave generation starts to be noticeable.

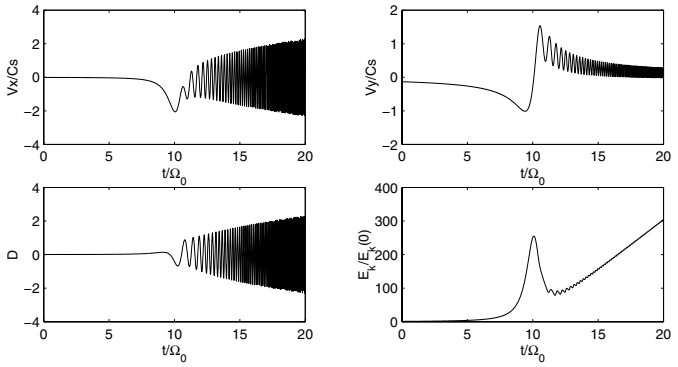

Fig. 2. The evolution of SFH normalized velocity and density perturbations (v_x/c_s, v_y/c_s, D) and its normalized energy ($E_{\boldsymbol{k}}(t)/E_{\boldsymbol{k}}(0)$) at $R_{\max} = 1.34$ ($m = 0.5R/H$ in terms of the azimuthal wavenumber). Evolving in the shear flow, the initially imposed vortex mode SFH (with $k_x(0)/k_y = -15$, $k_y = 0.5$), gaining energy from the mean flow and amplifying, retains its aperiodic nature until $k_x(t)/k_y < 0$. After time $t^* = 10$ (at which $k_y(10) = 0$), we observe the appearance of the wave SFH.

the vortex and wave SFH are comparable and the perturbations are not separable/distinguishable, i.e. we have a mix of SFH of aperiodic and oscillating modes. Subsequently, $R(t)$ becomes small again, the time scale of the wave SFH becomes much shorter than that of the vortex SFH and the modes become clearly distinguishable again.

In spite of what was said above, we carry out a separation of the modes also in the vicinity of time t^*, when $k_x(t^*) = 0$ and $R(t)$ is not small. The performed separation allows us to establish the initial characteristics of the generated wave SFH, that, in turn, determine the further dynamics/energetic of SFH, even quantitatively.

In Fig. 3 we present separately the dynamics of v_y/c_s, v_x/c_s, D and of their vortex ($v_y^{(v)}/c_s$, $v_x^{(v)}/c_s$, $D^{(v)}$) and wave components ($v_y^{(w)}/c_s$, $v_x^{(w)}/c_s$, $D^{(w)}$) for a pure vortex/aperiodic initial

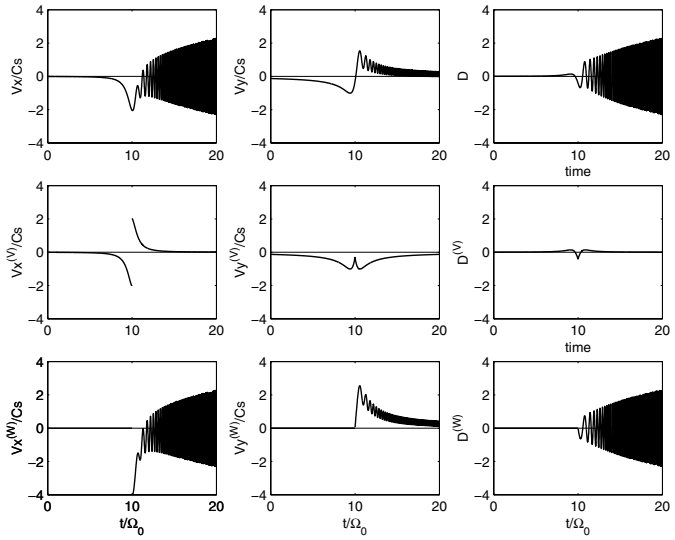

Fig. 3. The dynamics of v_x/c_s, v_y/c_s, D, their vortex ($v_x^{(v)}/c_s$, $v_y^{(v)}/c_s$, $D^{(v)}$) and wave parts ($v_x^{(w)}/c_s$, $v_y^{(w)}/c_s$, $D^{(w)}$) for a pure vortex initial perturbation ($v_x^{(w)}(0)$, $v_y^{(w)}(0)$, $D^{(w)}(0) = 0$) with the same parameters as in Fig. 2. The process may be interpreted as an abrupt emergence of wave SFH from the related vortex SFH at $t = t^*$. The amplitude of the generated wave $v_y^{(w)}(t^*)$ smoothes the jump in the aperiodic mode (see Eq. (39)).

perturbation ($v_y^{(w)}(0)$, $v_x^{(w)}(0)$, $D^{(w)}(0) = 0$), with the same parameters used for the case in Fig. 2. From Fig. 3 we notice:

- $v_y^{(v)}$ is an odd function of the argument $t - t^*$;
- $v_x^{(v)}$ and $D^{(v)}$ are even functions of the argument $t - t^*$;
- At time $t = t^*$, at which $k_x(t^*) = 0$, the vortex mode *abruptly* gives rise to the corresponding wave SFH (see Fig. 3, top panels);
- At the moment of wave SFH emergence, the phase is such that the value of $v_x^{(w)}(t \to t^*+)$, $D(w)(t \to t^*+) = 0$ and $v_y^{(w)}(t \to t^*+)$ is maximal (see Figs. 3, bottom panels). More precisely,

$$|v_y^{(w)}(t \to t^*+)| = 2|v_y^{(v)}(t \to t^*-)| = 2|v_y(t^*)|; \quad (39)$$

- The excited wave harmonic (satisfying condition $k_x(t)/k_y > 0$) gains energy from the shear flow and is amplified;
- The vortex SFH after the transient growth gives energy back to the background flow.

This process can be altered by the action of nonlinear forces, or by the presence of a radial entropy gradient in the Keplerian flow, in which case vorticity is continuously generated, feeding the vortex with Rossby waves (see Klahr 2004).

4. Qualitative study of Rossby waves

In the previous section we found that the compressible shearing sheet approximation results in a third order system of ordinary differential equations (see Eqs. (27)−(29)), or, equivalently, in a second order inhomogeneous differential equation (see Eq. (32)). This reduction is connected to the conservation of

potential vorticity and results in the fact that one of the perturbation modes is aperiodic/vortex. Consequently, the approximation involves two spiral-density waves propagating in opposite directions and one vortex mode. The vortex mode and spiral-density waves are no longer independent: they are coupled by the strong differential character of Keplerian rotation. As is shown in the previous section, the vortex mode unconditionally generates spiral-density waves, but the opposite does not occur, i.e. the waves do not a generate vortex/aperiodic mode.

A question arises: how does the picture change when the shearing sheet approximation is not valid, especially, when the mean vorticity gradient across the disk is at work? We consider this problem qualitatively, borrowing some estimates from Tagger (2001). At first, the linear dynamics of perturbations is described by a third order system of ordinary differential equations that, however, cannot be reduced to a second order inhomogeneous differential equation, as in the previous case. In this case all the perturbation modes are waves: two spiral-density and one Rossby wave. The frequency of the first ones is given by Eq. (35). We can get the frequency of the Rossby wave from Eq. (16) of Tagger (2001):

$$\omega_R(t) = \frac{k_y}{k_x^2(t)+k_y^2}\frac{\partial W}{\partial r} = -\frac{3}{4}\frac{\Omega}{r}\frac{k_y}{k_x^2(t)+k_y^2}. \quad (40)$$

From Eq. (40) it follows that in a thin ($H \ll r$) Keplerian disk, for perturbations with characteristic sizes of the order of the disk thickness ($k_x, k_y \simeq 1/H$), the Rossby wave frequency is much less than Ω. Considering a short time evolution ($\simeq 1/\Omega$), the disk thickness size Rossby waves represent a non-oscillating and non-propagating vortical perturbation. In practice, we have a degeneration of Rossby waves to vortex mode perturbations and for them the mean flow vorticity gradient can be neglected.

We present a simple sketch of the "breaking of the degeneracy" in the wavenumber plane (k_x, k_y) (see Fig. 4). The linear dynamics of a vortical perturbation may be described by following each of its SFH in the wavenumber plane. We single out a SFH that, initially, is located at point 1 in Fig. 4, for which $k_x/k_y < 0$; $k_y < 1/r$; $|k_x| \gg 1/r$., i.e. a tightly leading vortical perturbation with large azimuthal size. Formally, the perturbation represents a Rossby wave SFH. However, according to Eq. (40), its frequency is substantially smaller than Ω. Thus, the SFH is aperiodic, i.e., it is degenerated to a vortex mode SFH. According to Eq. (22), as $k_x(t)$ varies in time, the SFH drifts in the direction marked by the arrows (we present the drift of the SFH only in the upper half-plane $k_y > 0$; since the perturbation is real, there is a counterpart in the lower half-plane.) Initially, as $|k_x(t)|$ decreases, the energy of the SFH grows (see Figs. 1–3). Then, the SFH reaches the circled domain where $|k_y|/(k_x^2+k_y^2) < r$ (point 2) and its frequency becomes no longer negligible (the boundaries of the domain, where breaking of degeneracy occurs, are indistinct, but we fixed the domain to clarify the analysis). Thus, passing this domain, the SFH acquires a wave nature, i.e., the degeneration to a vortex mode is broken. At the same time, the Rossby wave SFH continues its growth that lasts until it crosses the line $k_x = 0$ (point 3). It then generates the related SFH of a spiral-density wave (as it does the vortex mode SFH – see Sect. 3). The drift after passing the line $k_x = 0$ is shown by the double line arrows to stress the appearance of the spiral-density wave SFH and its further drift equal to the Rossby wave drift. At point 4, the Rossby wave SFH leaves the circled domain and becomes tightly trailing, again degenerating into an aperiodic/vortex SFH. Thus, the Rossby wave appearance from a vortex mode perturbation is not connected to a generation process. The essence of the Rossby wave formation lies just in the "breaking of degeneracy" of the vortex mode perturbation. If we now choose a vortex mode SFH with $k_y > 1/r$ (e.g., at point 1′), it is not difficult to understand that the drifting SFH misses the circled domain and the breaking of degeneration never occurs, but, in crossing the line $k_x = 0$ (see point 3′), it generates its related spiral density wave SFH.

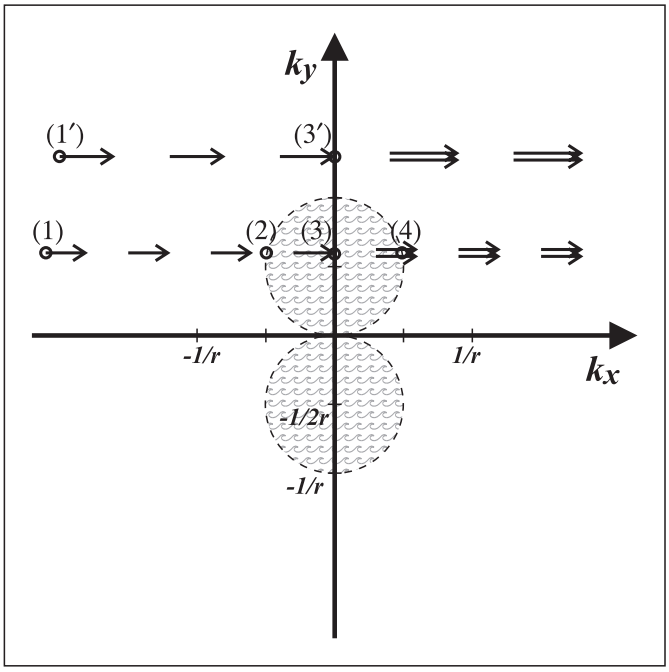

Fig. 4. Simple sketch of the relation between the Rossby wave and vortex mode perturbations in the wavenumber plane (K_x, K_y), see details in the text.

A supposition about the coupling of Rossby and spiral-density waves is expressed in Tagger (2001): "density waves generating Rossby waves as they propagate, and reciprocally Rossby waves spawning density waves as they are sheared by differential rotation". Chagelishvili & Chkhetiani (1995) investigated the linear dynamics of planetary atmospheric Rossby waves in the β-plane approximation, in a case of zonal flow. They found and described the generation of spiral-density waves by Rossby waves, but not the opposite. It may be that this asymmetry of the wave coupling is connected to the fact that in the system, we have only one Rossby and two spiral-density waves (propagating in opposite directions). The same asymmetry exists in case of wave and vortex mode coupling (see Sect. 3 and Chagelishvili et al. 1997). In this context it would be particularly interesting to consider the case where a radial entropy gradient is present (Klahr 2004), since in this

case there are two independent Rossby waves. The problem of Rossby wave generation by spiral-density waves in a given disk model (containing both angular velocity and vorticity gradients) will be the subject of a separate investigation.

5. Generation of spiral-density waves by coherent circular vortex structure – numerical simulations

5.1. Numerical setup

In this section we present 2D numerical simulations of Eqs. (1)−(5) in case of an initial coherent circular vortex perturbation superimposed on an equilibrium Keplerian flow.

Since the emphasis of our numerical simulations is not only on the vortex dynamics itself but also on the process of wave generation, we need initial conditions corresponding to the vortex perturbations in a pure form.

One of the ways to select the initial conditions for the vortex would be to employ an equilibrium vortex configuration. A class of widely used exact steady analytic solutions for single vortex patches is given by Saffman (1992). These solutions were also used for the construction of an elliptic vortex in Keplerian shear flow in numerical simulations by Chavanis (2000). Another class of time-dependent vortex solutions in uniform shear flows is given by Kida (1981). Stability analysis of the Kida vortex revealed some aspects of its non-modal behavior – transient growth due to the background velocity shear (see Meacham et al. 1990). However, these vortex configurations are solutions for incompressible flows and cannot be directly used in the compressible setup initially preserving the no-wave condition.

An exact equilibrium vortex solution in Keplerian shear flow is given by Goodman et al. (1987). However, the specificity of this solution is that it has a non-divergent velocity field, yielding a particular enthalpy distribution to balance the compressibility effects. In this sense, this vortex is not purely kinematic by nature, but involves thermodynamic forces in the equilibrium configuration.

Our aim is to perform numerical simulations of vortex dynamics for a direct comparison and verification of results obtained within the non-modal analysis in the wave-number space. For this purpose, we need an initial vortex configuration which will persist in a medium with constant sound speed – a property which is not valid for the equilibrium vortex derived by Goodman et al. (1987). Hence, we provide the algorithm for the construction of a pure vortex structure in compressible shear flow.

For simplicity we chose the initial vortex to be circular in shape having in mind that it will be sheared into an elliptical configuration during the evolution in the shear flow. The compressibility effects on vortex perturbations in flows with moderate shear parameters (as in Keplerian disks) are appreciable at $|k_x/k_y| \leq 1$, while the circular vortex we want to construct contains SFH from this domain of the wave-number space. Therefore, in this case we need a refined procedure to construct pressure, density and velocity fields that correspond to the vortex mode perturbations in a pure form. For this purpose we use "pre-initial" conditions for the perturbations in as follows:

$$v'_x(x,y,0) = \pm\epsilon_r \frac{y}{a}\left(\frac{x^2+y^2}{a^2}\right)^n \exp\left[-(x^2+y^2)/a^2\right], \quad (41)$$

$$v'_y(x,y,0) = \mp\epsilon_r \frac{x}{a}\left(\frac{x^2+y^2}{a^2}\right)^n \exp\left[-(x^2+y^2)/a^2\right], \quad (42)$$

$$\rho'(x,y,0) = 0, \quad (43)$$

where ϵ_r defines the amplitude of the perturbation, a its size, n the shape of the vorticity distribution and the upper and lower signs correspond respectively to anticyclonic and cyclonic rotation. Although the kinematics described by the above equations seems a pure vortex, this is not the case because the absence of the density disturbance denotes that the equations above describe a mixture of spiral density wave and vortical perturbations, with density disturbances fully compensating each other. We use them to describe a "pre-initial" condition, in the sense that through them we defined the distribution of $\mathcal{I}(k_x, k_y)$ in wavenumber plane. Then, on the basis of the procedure described in the Appendix, we constructed our actual initial condition, that is an almost pure (with minimal admixes of spiral-density waves) circular vortex with its corresponding density field. The velocity field of our initial disturbance has somewhat changed with respect to the "pre-initial" one. Our initial vortical perturbation represents a rich ensemble of leading ($k_x/k_y < 0$) and trailing ($k_x/k_y > 0$) harmonics, but only the presence of leading SFH sets the conditions for the generation of spiral-density waves.

We have then superimposed this perturbation on the equilibrium Keplerian flow and have performed the simulations using our implementation of the PPM scheme in its Eulerian version (Woodward & Colella 1984; Mignone et al. 2004). The main characteristics of the scheme are a parabolic reconstruction that gives third order spatial accuracy in smooth regions of the flow, a nonlinear Riemann solver and time advance based on a characteristic projection that is second order accurate. We have not used an angular momentum conserving form of the ϕ component of the momentum equation, however, we have tested that the total angular momentum is conserved by our code during the simulations, with a relative accuracy of 10^{-5}. For long-term simulations, e.g. hundreds of orbits, one would have to use a scheme that conserves the local angular momentum density (Kley 1998), but, as we only study the evolution of 2.5 orbits and only impose a linear perturbation, it is possible to neglect the precise angular momentum conservation. Since in this problem there are no natural units of length, we have arbitrarily chosen our unit of length as the radius at which the vortex center is located. The unit of velocity is then chosen as the Keplerian velocity v_{kv} computed at this radius, i.e. at $r = 1$, and the disk density is taken as units of density. In these units the computational domain covers the region $0.056 < r < 1.94$ and $0 < \theta < 2\pi$, in polar coordinates, with a uniform (both in r and in θ) grid of 1024×1024 points. We had to use such a number of grid points in order to have a good resolution on the vortex also covering a large area of the disk. In this way, for example, in the case with $a = 0.1$, we cover the vortex with about 100 points. The center of the vortex perturbation is then located at $r = 1$

Table 1. Parameters of the simulations and estimated values of other nondimensional parameters at the initial vortex position. For comparison we also give values of some parameters for Godon & Livio (1999) and Davis (2002) simulations.

	$c_s/v_{kv}\,(=H/r)$	a	n	$\Delta d/r$	$\Delta d/H$	v_M/V_{Kep}	N
A	0.26	0.1	0	0.25	1	0.0034	0.054
B	0.08	0.1	0	0.25	3.1	0.0034	0.054
C	0.26	0.01	0	0.025	0.1	0.00034	0.054
D	0.26	0.1	2	0.5	2	0.0015	0.015
Godon & Livio (1999)	0.15	–	–	0.05	0.33	0.03	2.4
Davis (2002)	0.075	–	–	0.25	3.3	0.08	1.3

and $\theta = \pi/4$. In our units, the rotation period at the location of the vortex is therefore $T = 2\pi$ and our simulations reach time $t = 2.5T$. Boundary conditions are periodic in the azimuthal direction and outflow in the radial direction. More precisely, in the radial direction we impose the zero-derivative of all the quantities, except the azimuthal velocity, for which we continue the Keplerian profile and impose the zero-derivative on the perturbation. These conditions do not ensure perfect transmission of perturbations impinging on the boundaries, however the portions of perturbation that are reflected at the boundaries become leading waves that are deamplified by the shear and can influence only a small region close to the boundaries. The main parameters of our system are then c_s, a, ϵ_r and n (see Eqs. (41)−(43) above). We have considered two values of the sound speed, two sizes of the vortex and two values for n. In Table 1 we report the values of the parameters used in our simulations together with some other nondimensional parameters that may help in comparing the importance of different effects on the vortex dynamics. For comparison, in the table we reported the same parameters for the simulation performed by Godon & Livio (1999) and Davis (2002).

The second column in Table 1 gives the value of the sound speed (in units of the Keplerian velocity v_{kv} at the position of the center of the vortex) and, according to Eq. (10) this is equivalent to the values of the ratio H/r between the disk thickness and the radius. Case B clearly represents the case with the lowest value of H/r, however all the cases help to gain more insight into the dependence of the vortex dynamics on the parameters: a comparison between case A and case B allows us to investigate the effect of the sound speed, case C allows us to investigate the effect of the vortex size and case D allows us to investigate the effect of a different vorticity distribution (a value of n different from 0 gives a vorticity ring, while $n = 0$ gives a filled distribution). Unlike what we said above, in case C we made use of 1096×4192 grid points covering the domain $0.5 < r < 1.5$ and $0 < \theta < \pi/2$ and the final integration time is $t = 3.5$. With this choice we could keep the same resolution on the vortex that we have for the other cases. The amplitude of the perturbation in all cases, except case C, is $\epsilon = 0.004$, and in case C it is ten times smaller, in order to minimize the action of nonlinear terms of Eqs. (1)−(4), since in this paper we want to address the linear dynamics of the perturbation. We do this to prove the linear character of the spiral-density wave generation process (the main aim of our study) and to visualize the wave generation and propagation processes clearly. In the linear case there is no difference between the dynamics of cyclonic and anticyclonic vortices, so, without loss of generality we took the vortex rotation to be anticyclonic.

The parameters $\Delta d/r$ and $\Delta d/H$, as discussed in Sect. 4, giving the vortex core size Δd in units respectively of the radius and of the disk thickness, measure the importance of the Rossby waves. On the basis of Eq. (40) one can estimate the characteristic oscillation times of the Rossby waves in the simulated cases. These times significantly exceed the time of our simulation – a few revolutions of the disk at the vortex location. Consequently, Rossby waves do not manifest themselves in our simulations, i.e., the real participants of the simulated dynamics are the vortex mode and the (generated) spiral-density wave.

The parameter N in the last column of Table 1 measures the competition between the distortion by the shear flow (linear phenomenon) and nonlinear phenomenona that might oppose this distorsion. This competition may be estimated by the ratio between the vortex maximum velocity v_M and the local Keplerian velocity difference across the vortex core radius ($|\partial V_{Kep}/\partial r|\Delta d/2$)

$$N = \frac{v_M}{|\partial V_{Kep}/\partial r|\Delta d/2} = 4\frac{v_M}{V_{Kep}}\frac{r}{\Delta d}. \tag{44}$$

At $N \ll 1$ the vortex dynamics is completely linear; when N becomes of the order of unity or larger, nonlinear effects are important. As one can see from the table, the value of this parameter for Godon & Livio (1999) and Davis (2002) indicates that in their simulations nonlinear effects are important, while all our cases describe strongly linear dynamics of vortices.

5.2. Results

In Fig. 5 we represent the initial conditions of our simulations (for $n = 0$), more precisely we show the vorticity (upper panel) and density (lower panel) perturbation fields, with enlargements of the vortex region. The vorticity field of the initial vortical perturbation has axial symmetry, as expected, while the density field has a different structure resulting from the balance of pressure and Coriolis forces. In Figs. 6 and 7, we show the initial phases of the vortex evolution for case A, up to $t = 2\pi$, that corresponds to one rotation period at the initial vortex location. The figures show respectively images of vorticity and density distributions at six different times. We see that the vortex

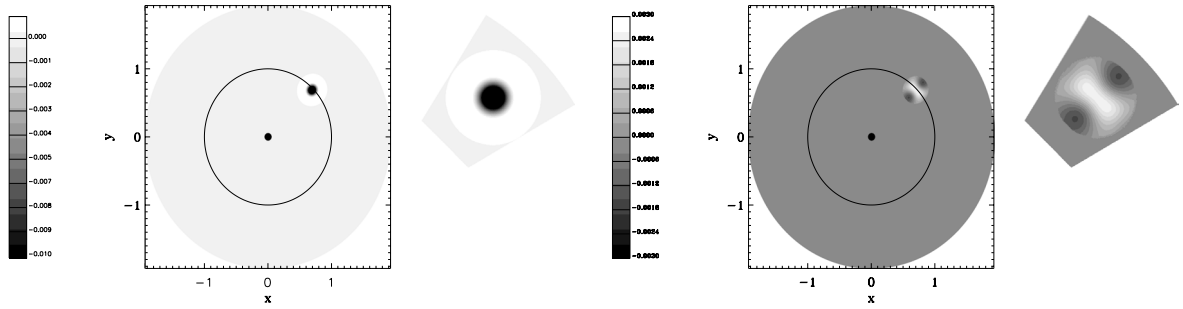

Fig. 5. Images of the initial density (*left plot*) and vorticity (*right plot*) distributions with enlargements of the vortex area.

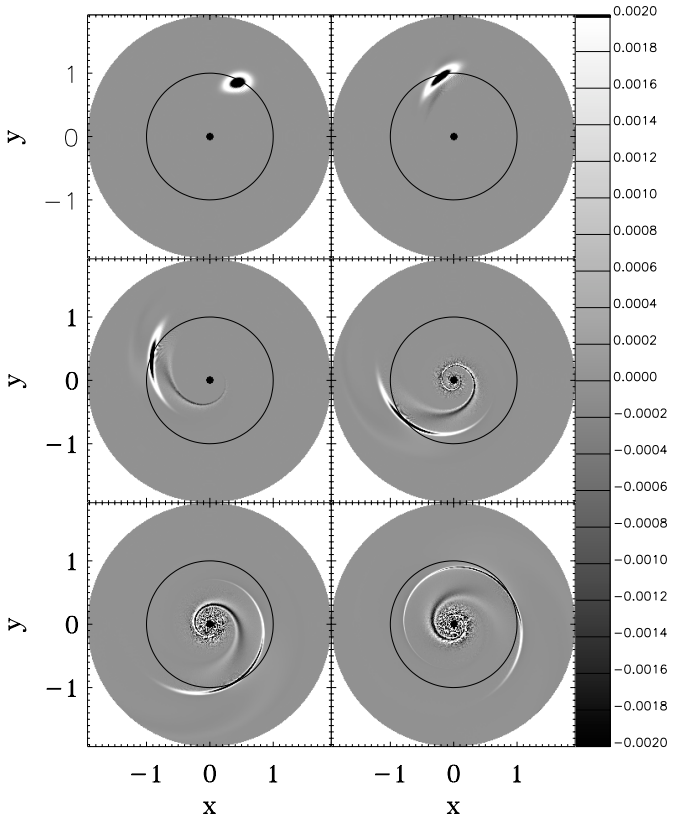

Fig. 6. Evolution of the vorticity distribution for case A. The six panels show the vorticity distributions at six different times. The times are respectively $t = 0.31, 1, 2, 3.12, 4.5, 6.31$. At late times the vorticity distribution in the inner region becomes quite noisy, however one has to take into account that the calculation of vorticity implies a numerical differentiation operation that amplifies the error, larger here due to the grid deformation

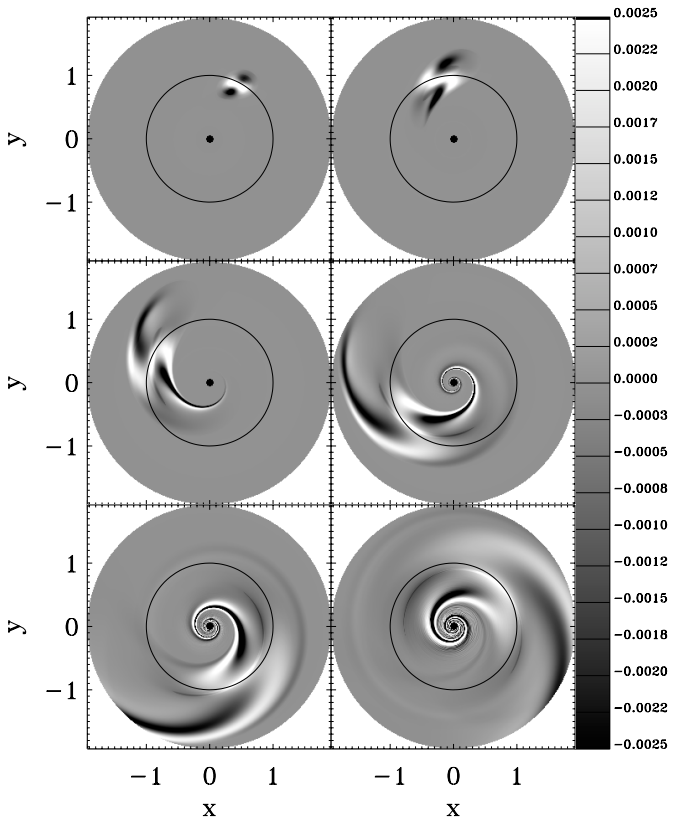

Fig. 7. Evolution of the density distribution for case A. The six panels show the density distributions at six different times, $t = 0.31, 1, 2, 3.12, 4.5, 6.31$.

is stretched by the background Keplerian flow, but we can also observe that, in agreement with the theory presented in Sect. 3, two spiral-density waves are being generated by the vortex. The stretching is well visualized in Fig. 6, that shows the vorticity dynamics. The wave generation and propagation phenomena are well traced by the two arms that are visible on the images of Fig. 7. According to what we have shown in previous sections, a vortex SFH generates a wave when the SFH crosses the k_y axis, i.e. when the wavenumber in the local radial direction becomes zero ($k_x = 0$, see Fig. 3 and points 3 and 3′ in Fig. 4). Our vortex is composed of many SFH, and each of them, crossing the k_y axis, generates the corresponding spiral-density wave SFH component. Therefore, since at the moment of generation the wavenumber is along the azimuthal direction, we can observe the two generated waves to be propagating in opposite azimuthal directions. The waves, as they propagate, have their wavevectors turned by the shear flow towards the radial direction, and in time they are carried by the flow and become tightly trailing. The appearance of two arms is related to the conservation of the perturbation action, that initially is zero, since the vortex perturbation does not propagate. The total action of the generated wave arms should then be zero and therefore we have two arms with opposite propagation directions.

We now define and compute the trajectories of the excited spiral-density waves by using the group velocity concept (of course, trajectory, as wave group velocity, gains in importance

only for wave packages when the concept of ray is applicable). The trajectories that we will compute will be global, but they will be based on the local dispersion relation that can be obtained at each position in the shearing-sheet approximation. The validity of the trajectories that we will compute has therefore all the limitations of this approximation. Due to this "half-globality" we will indicate by $k_r(t)$ and k_θ (instead of $k_x(t)$ and k_y that are used in the local reference frame) the components of the wavenumber vector respectively in the local radial and azimuthal directions. We rewrite the dispersion relation of spiral-density waves from Eq. (34)

$$\begin{aligned}\omega_{\rm s}(k_r(t),k_\theta) &= \pm\left[\Omega^2+(k_r^2(t)+k_\theta^2)c_{\rm s}^2\right]^{\frac{1}{2}}\\ &= \pm\left[1+H^2(k_r^2(t)+k_\theta^2)\right]^{\frac{1}{2}}c_{\rm s}\end{aligned} \tag{45}$$

and then we obtain from it the radial and azimuthal components of the group velocity

$$\boldsymbol{V}_{\rm s}^G = \left(\frac{\partial\omega_{\rm s}}{\partial k_r(t)}\,,\,\frac{\partial\omega_{\rm s}}{\partial k_\theta}\right) = \left(\pm\frac{k_r(t)c_{\rm s}}{\sqrt{1+H^2[k_r^2(t)+k_\theta^2]}},\right.$$
$$\left.\pm\frac{k_\theta c_{\rm s}}{\sqrt{1+H^2[k_r^2(t)+k_\theta^2]}}\right). \tag{46}$$

The two signs identify the two oppositely propagating spiral-density waves. We notice that the group velocity is time-dependent as $k_r(t)$ depends on time. We can now compute the trajectory by defining the total wave velocity as

$$\frac{{\rm d}\boldsymbol{r}_{\rm s}}{{\rm d}t} = \boldsymbol{V}_{\rm s}^T = \boldsymbol{V}_{\rm s}^G + \boldsymbol{V}_k \tag{47}$$

with the wavenumber that changes according to the equation

$$\frac{{\rm d}k_r(t)}{{\rm d}t} = -2A(r)k_\theta, \tag{48}$$

where $A(r)$ is local value of the Oort's constant. As discussed in Sect. 3, the group velocity of spiral-density waves is directed along the azimuthal direction at the moment of their generation, i.e., initially we observe two oppositely propagating rays in this direction. We can then follow the propagation by numerically integrating Eqs. (47)−(48). In Figs. 8 and 9 we plot the trajectories that we have obtained in this way, superimposed on the results of the full numerical simulations at time $t = 2$ for the two cases A and C that differ for the initial vortex size. The different trajectories correspond to different values of k_θ at the emission time. The trajectories have a characteristic S-shape since the two rays oppositely propagating in the azimuthal direction are progressively turned towards the radial direction and in the meantime they are carried by the background Keplerian flow. We can see that our computed trajectories agree quite well with the results of numerically simulated propagation of spiral-density waves. We see that the agreement is better for the case with an initially smaller vortex size. In both cases we have part of the perturbation that is ahead of the computed trajectory, but this part is larger for case A. This partial disagreement can be considered as the result of the breakdown of the approximations used in computing the trajectories and of course, the approximations are better for a smaller size vortex.

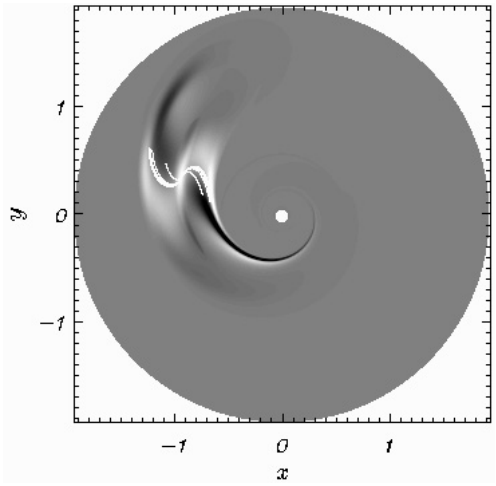

Fig. 8. Ray trajectories superimposed on the density distribution for case A at time $t = 2$. The different rays correspond to different values of k_θ.

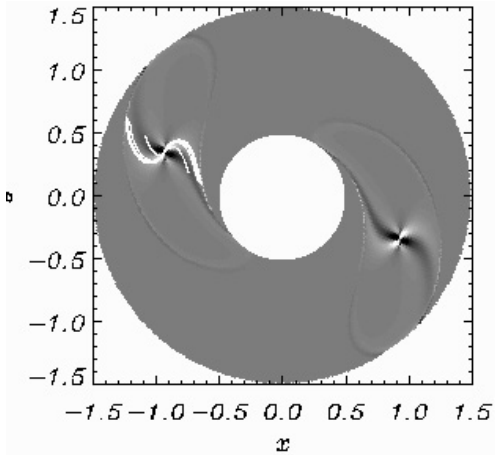

Fig. 9. Ray trajectories superimposed on the density distribution for case C at time $t = 2$. The different rays correspond to different values of k_θ. In the image we show also a vortex in a symmetric position for better comparison. Note that in case C the computational domain covers the radial interval $0.5 < r < 1.5$.

In Fig. 10 we again plot trajectories and numerical simulation results for case A at a later time ($t = 3.75$), to show that the computed trajectories follow with a very good agreement the further perturbation evolution.

Figure 7 show a very regular structure of the emitted spiral-density waves. *Prima facie*, they look like shocks, but this is not the case. They have a *linear origin* and we can understand the observed regular structure as described below. A wide spectrum of wave SFH is generated at each moment of time, since the intensity of generation is different from zero over a wide range of k_y (see Sect. 3), and the panels in Fig. 7 represent an integral picture of the generated and propagating wave interference. On the other hand, according to the graphs of $v_x^{(\rm w)}$, $v_y^{(\rm w)}$, $D^{(\rm w)}$ in Fig. 3, the wave harmonics, at the moment of generation, have very regular phases that are similar to each other (specifically, all density perturbation SFH are excited with zero phase – see

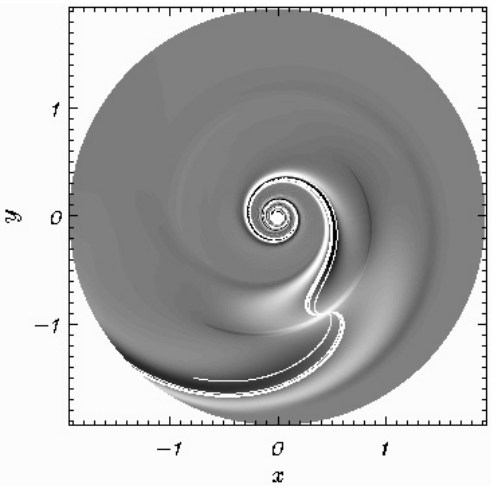

Fig. 10. Ray trajectories superimposed on the density distribution for case A at time $t = 3.75$. The different rays correspond to different values of k_θ.

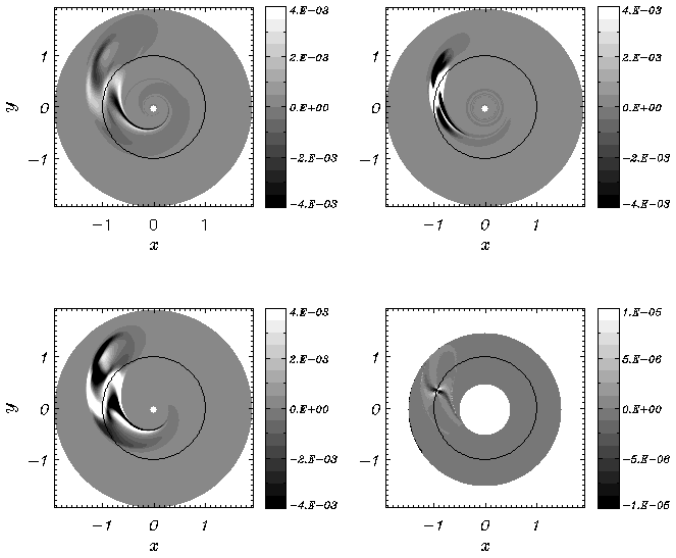

Fig. 11. Comparison of the four different cases at the same time. The four panels show images of the density distribution for cases A (*top left*), B (*top right*), C (*bottom right*) and D (*bottom left*) at $t = 2$.

graph of $D^{(\mathrm{w})}$ in Fig. 3). This phase regularity and similarity are the roots of the regular interference picture shown in Fig. 7.

In vortical flows, potential perturbations acquire a vortical nature and this is the case for the spiral-density waves that we are considering. We can estimate the wave vorticity by Eq. (29), rewritten in a "half-global" fashion (as was done defining trajectories). For spiral density waves we have $\mathcal{I} = 0$:

$$k_r(t)v_\theta^{(\mathrm{w})}(t) - k_\theta v_r^{(\mathrm{w})}(t) + 2[\Omega(r) + A(r)]D^{(\mathrm{w})}(t) = 0. \tag{49}$$

Defining the wave SFH vorticity as

$$W^{(\mathrm{w})} \equiv k_r(t)v_\theta^{(\mathrm{w})}(t) - k_\theta v_r^{(\mathrm{w})}(t), \tag{50}$$

we finally get:

$$W^{(\mathrm{w})}(t) = -\frac{1}{2}\Omega(r)D^{(\mathrm{w})}(t). \tag{51}$$

From this equation we can see that the vorticity of the propagating wave is determined by the local vorticity of the background flow and by the amplitude of the density perturbation. Both factors grow for the wave propagating towards the inner part of the disk and the result is an increase of the wave vorticity in this region. For the outward propagating wave, instead, the density amplitude still increases but at a much lower rate than the decrease of the background flow vorticity. Therefore the net result will be a decrease of its vorticity. This asymmetry is well traced in Fig. 6, where we see a vanishing of the outward arms, while the inward ones become well pronounced.

In Fig. 11 we show grey-scale images of the density distribution at $t = 2$ for the cases A, B, C, D. Cases A and D relate to equal sizes of parent vortex and sound speeds (see Table 1, they differ only for the values of n) and the wave propagation pictures are very similar. In case B, due to the small value of the sound speed, the wave arms are radially compressed and not strongly pronounced. In case C, due to the small size of the parent vortex, the generated wave SFH has large wavenumbers, their group and phase velocities are more or less the same (close to the sound speed) and the arms are more uniform (not diffuse).

Due to linearity, the described phenomena have a short life time (a few disk revolutions): in fact vortex distortion by the background shear flow cannot be prevented by velocity self-induction (a nonlinear phenomenon). The parent vortex is stretched, becomes tightly trailing (see Fig. 6) and, in accordance with Sect. 3, is not able to generate any more spiral-density waves. Also, the trailing vortex mode perturbations ($k_x(t)/k_y > 0$) give back energy to the flow and disappear (also in accordance with Sect. 3). The disappearance of the parent vortex is evident in Fig. 12, where we show grey-scale images of density at later evolution times; the three panels are respectively at $t = 8.12, 11.25, 14.5$, i.e. up to two and a half revolutions. Spiral-density tightly trailing waves have extended to the whole disk region inside the vortex position, but their generation seems to have stopped and they have disappeared from the outer region.

Preliminary results show that nonlinearity makes the parent vortex long-lived and the wave generation process more permanent (Bodo et al. 2005). Indeed, prevention of parent vortex stretching should be the result of positive nonlinear feedback, i.e. nonlinear regeneration of the leading SFH in the vortex spectrum. These replenished leading SFH extract the disk flow energy and generate continuously spiral-density wave SFH. Consequently, they provide a permanent generation of waves. (The concept of replenishing of SFH – a root of the positive nonlinear feedback – is a theoretical concept, numerical investigation of which is under way).

The results for a single Fourier component, given in Sect. 3, show that the energy of the generated spiral density wave increases with time, i.e. trailing spiral density waves are capable of extracting energy from the mean flow. This wave amplification should also be visible in our numerical calculations; for this reason, in Fig. 13, we plot the perturbation energy (as defined in Eq. (31)) vs. time.

In the figure we can see the perturbation normalized energy (normalized to the initial value) vs. time for the cases A,

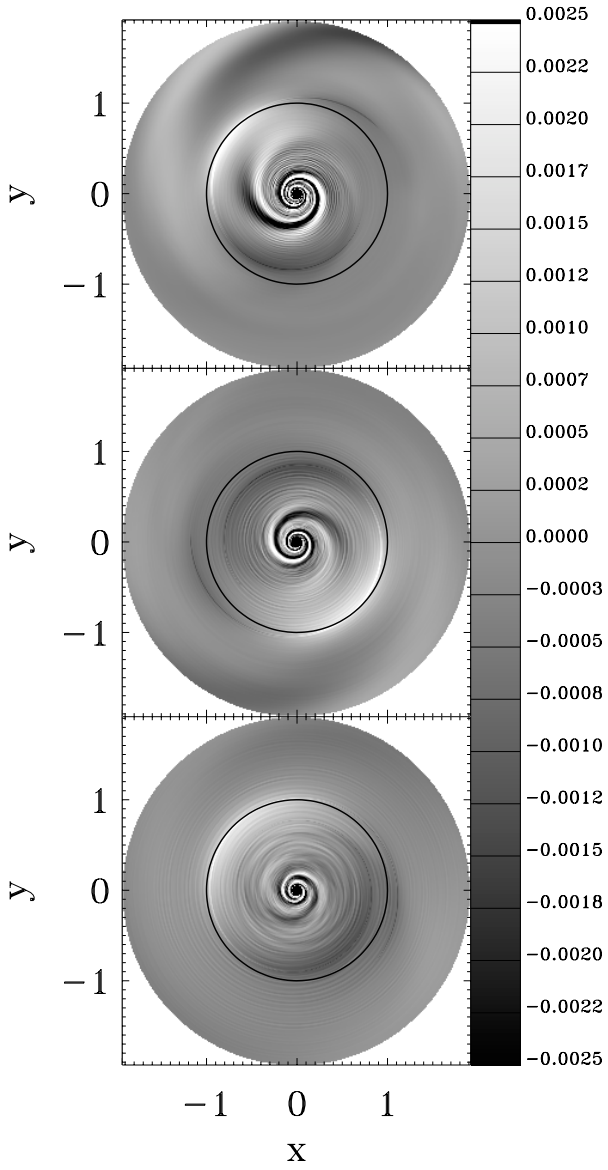

Fig. 12. Longer time evolution for case A. The three panels show images of the density distributions at three different times; from top to bottom the times are respectively $t = 8.12, 11.25, 14.5$.

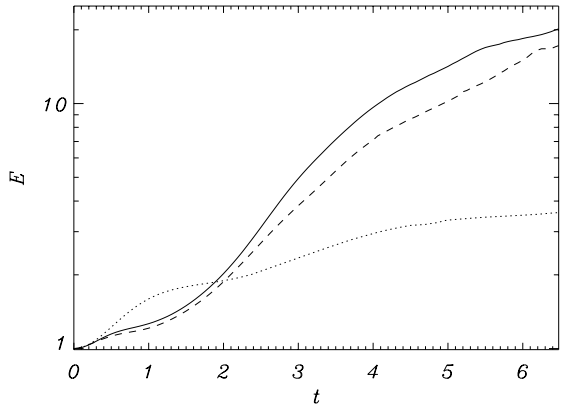

Fig. 13. Energy normalized to the initial value versus time for the cases A, B and D (the solid line refers to case A, the dotted curve to case B and the dashed curve to case D).

B and D (case A – solid curve, case B – dotted curve, case D – dashed-dotted curve). The plots go up to one revolution time ($t_{\max} = 2\pi$), when the action of the parent vortex has not yet completely disappeared. In this process of wave generation, the vortex acts only as a mediator and the waves draw their energy from the background flow, both at the beginning, when they are generated, and in their propagation, when they are amplified by the background shear flow. $k_r(t)$ of the generated wave SFH increases with time and the dynamics of SFH becomes adiabatic, therefore the energy of each SFH increases linearly with its frequency: $E_{\boldsymbol{k}} \sim \omega_{\rm SD}$. Generally, according to Eq. (35)

$$\omega_{\rm SD}^2 = \Omega^2 + \left[k_r^2(t) + k_\theta^2\right] c_{\rm s}^2, \tag{52}$$

but, at moderate sound speeds (cases A and D), in Eq. (52) the second term becomes quite rapidly dominant and, as time passes, one can write $E_{\boldsymbol{k}} \sim k_r(t) c_{\rm s}$, i.e. the energy of each SFH increases linearly with time. The increase of k_r is determined by the local shear rate, that increases in the inner region, at smaller values of the radius r. It is easily understood that at low sound speeds (case B) in Eq. (52) the first term is dominant for a long time and moreover the increase in k_r is slower, since the waves propagate more slowly towards the interior and they therefore experience a smaller shear rate. Consequently, $\omega_{\rm SD}$ and $E_{\boldsymbol{k}}$ are practically constant.

A feature of the generated spiral density waves that we have discussed above is their regularity, i.e. perturbations associated with the waves have a prominent sign and do not average to zero. One consequence of this is that, in principle, it may be possible to have a mass flux associated with them, that would be therefore proportional to the wave amplitude. We have tested this possibility by plotting the function:

$$Q(r,t) = \frac{1}{2\phi} \int_0^t {\rm d}t' \int_0^{2\pi} {\rm d}\theta \rho v_r(r,\theta,t') \tag{53}$$

as a function of time, at different radial positions ($r = 0.875$ and $r = 1.125$ in Fig. 14, $r = 0.1$ in Fig. 15). This function $Q(r,t)$ represents the total mass that has flown through radius r at time t, in units of the mass contained inside the initial vortex radial position. Figure 14 represents this quantity for positions that are immediately inside ($r = 0.875$, dashed line) and immediately outside ($r = 1.125$, solid line) the vortex. The figure shows that the action of the waves seems to be in the direction of mass collecting towards the vortex area. Figure 15 represents, instead, the mass flow induced by the waves in the inner disk region (at $r = 0.1$). Here we see a definite tendency of the wave to induce a non-negligible inflow of mass. These plots suggest a general trend of the phenomenon. and more realistic results with simulation of longer time dynamics of large amplitude coherent vortices are needed (Bodo et al. 2005). As discussed above, since we are essentially considering a linear process and since the quantity $\mathcal{M}$ is a first order quantity, the values that we get are proportional to the initial amplitude of the perturbation we give. The case that we present is an anticyclonic vortex; simulations of a cyclonic vortex show that all the fluxes are reversed, as they should be. Of course, in addition to this mass flux that is proportional to the perturbation

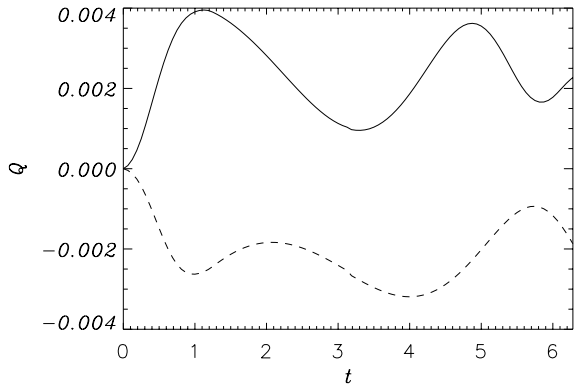

Fig. 14. Plot of the total mass that has flown through radius r at time t versus time, for case A. This figure refers to radial positions that are immediately inside ($r = 0.875$, solid line) and immediately outside ($r = 1.125$, dashed line) the vortex.

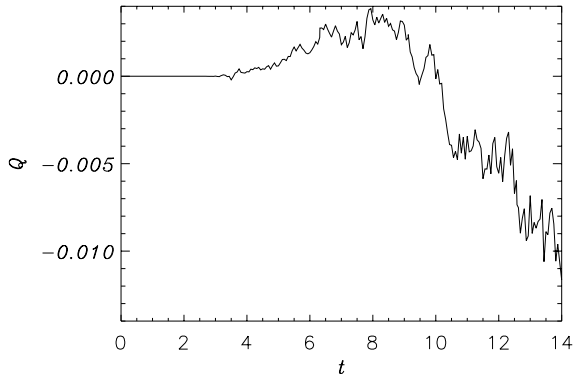

Fig. 15. Total mass that has flown through radius r at time t versus time, for case A. This figure refers to $r = 0.1$.

amplitude, the trailing spiral density waves induces an outward angular momentum transfer that is quadratic in the perturbation amplitude and, therefore, negligible in these linear calculations.

6. Discussion and conclusions

In this paper we present a linear, non-resonant phenomenon of spiral-density wave generation by vortices in a Keplerian disk flow that is closely related to the non-normality of linear dynamics of perturbations in smooth (without inflection points) shear flows. This phenomenon can be well interpreted by the use of the non-modal approach, i.e. by following in time the linear dynamics of spatial Fourier harmonics of the vortex mode perturbations. We have done this in the shearing sheet model and we found that spiral-density wave are generated only by the leading vortex mode SFH that meet the condition $k_x(0)/k_y < 0$. The generation takes place at relatively large wavelengths of SFH – it becomes noticeable at about $k_y H \simeq 0.7$ and it is dominant in the SFH dynamics at $k_y H < 0.5$. At large wavenumbers (small wavelength) all dynamics of SFH runs at low shear rates and only one phenomenon occurs: transient growth of SFH of aperiodic vortices. At small wavenumbers (large wavelength) when $k_y H < 0.5$, the dynamics in addition to the transient growth involves conversion of vortices to spiral-density waves. After their appearance, the energy of the wave SFH increases and the wave SFH itself in time becomes tightly trailing $k_x(t)/k_y \gg 1$.

Small amplitude (linear) circular vortex structures (that represent a rich ensemble of leading and trailing SFH) generate two oppositely propagating wave arms in accordance with the perturbation action conservation law. They have very regular structure and *prima facie* look like shocks, but this is not the case. They have a linear origin and are the result of the interference of the generated spiral-density waves. Their outward and inward propagating arms are asymmetric due to the disk curved geometry and flow asymmetry ($\Omega(r)$ increases outward and decreases inward).

Since spiral-density wave generation is governed by linear forces, it does not depend on the sign of the vorticity of initial aperiodic perturbation and should be equal for cyclonic and anticyclonic vortices even in the nonlinear regime. Davis (2002) (whose simulations are in a nonlinear regime – see Table 2), reported that a coherent cyclonic vortex simultaneously emits a wave as does an anticyclonic one (nonlinear cyclonic and anticyclonic vortices differ by their lifetime – cyclonic vortices are destroyed in appreciably shorter times than anticyclonic ones). This result may be considered as circumstantial evidence for the linear origin of the wave.

The fact that the waves are generated by a linear mechanism (and not nonlinear ones, as was thought) appreciably increases the significance of waves in the disk matter inflow/outflow processes and we showed that waves generated by anticyclonic vortices tend to collect matter in the vortex region, which may be important for protoplanetary disks, and tend to induce inflow of matter in the inner disk regions.

The described dynamics are short-lived due to the small amplitude of the parent vortex. One can speculate that the parent vortex could be long-lived and the dynamical picture more permanent at larger amplitudes, when nonlinear self-induction of the vortex velocity prevents its shear distortion. Indeed, nonlinear regeneration of the leading SFH ($(k_x/k_y < 0)$) in the vortex spectrum can prevent the vortex from stretching. These replenished leading SFH gain the disk flow energy and continuously generate spiral-density wave SFH. Thus, permanent nonlinear replenishment of leading SFH of the parent vortex could generate permanent disk flow energy extraction and wave generation. The effective efficiency of the feedback mechanism in permanently maintaing the vortex and overcoming the linear and nonlinear damping effects inherent to a Keplerian disk (Hawley et al. 1999) however has still to be proven by numerical simulations and analytical means.

The linear phenomenon of spiral-density wave generation by vortices investigated in this paper is quite universal; it occurs in disk flows with high shear rates and should be seen in different kind of astrophysical disks (protoplanetary disks; quasars; thin and thick galactic and binary system disks).

Acknowledgements. This work is supported by ISTC grant G-553 and GRDF grant 3315 and by MIUR grant 2002028843. G.D.C. and A.G.T. would like to acknowledge the hospitality of Osservatorio Asrtonomico di Torino. Numerical calculations were partly performed in CINECA (Bologna, Italy) thanks to the support by INAF. The authors would like to thank H. Klahr for helpful comments that improved the paper.

References

Baggett, J. S., Driscoll, T. A., & Trefethen, L. N. 1995, Phys. Fluids, 7, 833

Barge, P., & Sommeria, J. 1995, A&A, 295, L1

Bodo, G., Chagelishvili, G., Murante, G., Tevzadze, A., & Rossi, P. 2005, in preparation

Bracco, A., Chavanis, P. H., Provanzale, A., & Spiegel, E. A. 1999, Phys. Fluids, 11, 2280

Chagelishvili, G. D., & Chkhetiani, O. G. 1995, JETP Lett., 62, 301

Chagelishvili, G. D., Tevzadze, A. G., Bodo, G., & Moiseev, S. S. 1997, Phys. Rev. Lett., 79, 3178

Chagelishvili, G. D., Tevzadze, A. G., Bodo, G., Rossi, P., & Gogoberidze, G. T. 2000, Vortex-wave conversion in high shear flows, in Advances in Turbulence. VIII, Barcelona, Spain, June 27−30, ed. by C. Dopazo (CIMNE, 2000), 737

Chagelishvili, G. D., Chanishvili, R. G., Hristov, T. S., & Lominadze, J. G. 2002, JETP, 94, 434

Chagelishvili, G. D., Zahn, J.-P., Tevzadze, A. G., & Lominadze, J. G. 2003, A&A, 402, 401

Chavanis, P. H. 2000, A&A, 356, 1089.

Chapman, S. J. 2002, J. Fluid Mech., 451, 35

Craik, A. D. D., & Criminale, W. O. 1986, Proc. R. Soc. London, Ser. A, 406, 13

Davis, S. S., Sheehan, D. P., & Cuzzi, J. N. 2000, ApJ, 545, 494

Davis, S. S. 2002, ApJ, 576, 450

Farrell, B. F., & Ioannou, P. J. 1993, Phys. Fluids, A 5, 1390

Farrell, B. F., & Ioannou, P. J. 2000, Phys. Fluids, 12, 3021

Fridman, A. M. 1989, Sov. Astr. Letters, 15, 487

Gebhardt, T., & Grossmann, S. 1994, Phys. Rev. E, 50, 3705

Godon, P., & Livio, M. 1999, ApJ, 523, 350

Godon, P., & Livio, M. 2000, ApJ, 537, 396

Goldreich, P., & Lynden-Bell, D. 1965, MNRAS, 130, 125

Goldreich, P., & Tremaine, S. D. 1978, ApJ, 222, 850

Goodman, J., Narayan, R., & Goldreich, P. 1987, MNRAS, 225, 695

Grossmann, S. 2000, Rev. Mod. Phys., 72, 603

Gustavsson, L. H. 1991, J. Fluid Mech., 224, 241

Hawley, J. F., Balbus, S. A., & Winters, W. F. 1999, ApJ, 417, 361

Henningson, D. S., & Reddy, S. C. 1994, Phys. Fluids, 6, 1396

Ioannou, P. J., & Kakouris, A. 2001, ApJ, 550, 931

Johansen, A., Andersen, A. C., & Brandenburg, A. 2004, A&A, 417, 361

Kida, S. 1981, J. Phys. Soc. Japan, 50, 3517

Klahr, H., & Bodenheimer, P. 2003, ApJ, 582, 869

Klahr, H. 2004, ApJ, 606, 1070

Kley, W. 1998, A&A, 338, 37

Li, H., Finn, J. M., Lovelace, R. V. E., & Colgate, S. A. 2000, ApJ, 533, 1023

Lominadze, J. G., Chagelishvili, G. D., & Chanishvili, R. G. 1988, Sov. Astr. Lett., 14, 364

Lovelace, R. V. E., Li, H., Colgate, S. A., & Nalson, A. F. 1999, ApJ, 513, 805

Meacham, S. P., Flierl, G. R., & Send, U. 1990, Dyn. Atm. & Oceans, 14, 333

Mignone, A., Massaglia, S., & Bodo, G. 2004, Ap&SS, 293, 199

Nakagawa, Y., & Sekiya, M. 1992, MNRAS, 256, 685

Reddy, S. C., Schmid, P. J., & Henningson, D. S. 1993, SIAM J. Appl. Math., 53, 15

Saffman, P. G. 1992, Vortex Dynamics (Cambridge Univ. Press)

Tagger, M. 2001, A&A, 380, 750

Tevzadze, A. G., Chagelishvili, G. D., Zahn, J.-P., Chanishvili, R. G., & Lominadze, J. G. 2003, A&A, 408, 779

Online Material

Appendix A: Selection of initial values of vortex mode perturbations

The initial values of physical quantities for our two dimensional direct numerical simulations of Eqs. (1)−(4) may be composed by the superposition of the background flow and local vortex mode perturbation centered at some r_0:

$$\boldsymbol{V}(r,\phi,0) = \boldsymbol{V}_0(r,\phi,0) + \boldsymbol{v}'(x,y,0), \tag{A.1a}$$

$$P(r,\phi,0) = P_0 + p'(x,y,0), \tag{A.1b}$$

$$\rho(r,\phi,0) = \rho_0 + \rho'(x,y,0). \tag{A.1c}$$

where x and y is defined by

$$x \equiv r - r_0; \quad y \equiv r_0(\phi - \Omega_0 t); \quad \frac{x}{r_0}, \frac{y}{r_0} \ll 1. \tag{A.2}$$

The background is the Keplerian flow ($\boldsymbol{V}_0 = (0, V_{0\phi}, 0)$, $V_{0\phi}^2(\boldsymbol{r}) = GM/r$) with homogeneous pressure and density (P_0, ρ_0 = const.). The rigorous selection of initial vortex mode perturbation in the (compressible) flow requires a refined procedure, as vortex (aperiodic) modes acquire nonzero divergence – nonzero density perturbation (see discussion in Sect. 3). In order to select initial vortex mode perturbations we use the initial value problem in the wavenumber plane ($\boldsymbol{k}$-plane):

$$\begin{pmatrix} v_x'(x,y,0) \\ v_y'(x,y,0) \\ \rho'(x,y,0) \\ p'(x,y,0) \end{pmatrix} = \int\int \mathrm{d}k_x \mathrm{d}k_y \begin{pmatrix} v_x(k_x,k_y,0) \\ v_y(k_x,k_y,0) \\ \varrho(k_x,k_y,0) \\ p(k_x,k_y,0) \end{pmatrix} \times \exp(\mathrm{i}k_x x + \mathrm{i}k_y y). \tag{A.3}$$

Rewriting Eqs. (29), (31):

$$\frac{\mathrm{d}^2 v_y(t)}{\mathrm{d}t^2} + \left[4\Omega_0(\Omega_0 + A) + k^2(t)c_\mathrm{s}^2\right] v_y(t) = k_x(t) c_\mathrm{s}^2 \mathcal{I}, \tag{A.4}$$

$$k_x(t)v_y(t) - k_y v_x(t) + 2(\Omega_0 + A)D(t) = \text{const.} \equiv \mathcal{I}. \tag{A.5}$$

Hence, $\mathcal{I}$, $v_y(0)$ and $\left[\mathrm{d}v_y(t)/\mathrm{d}t\right]_{t=0}$ form the full set of initial conditions for Eq. (A.4). We seek the vortex mode solution in the following analytic form:

$$v_y(0) \equiv v_0(0) + v_1(0) + \ \ldots\ + v_n(0) + \ \ldots, \tag{A.6}$$

where the zero order term is deduced from the stationary form of the solution (see Eq. (A.4) at $A = 0$) and subsequent terms are derived using the iterative method (see also Chagelishvili et al. 1997):

$$v_0(0) \equiv [v_0(t)]_{t=0} \equiv \left[\frac{k_x(t)}{\mathcal{K}}\right]_{t=0} \mathcal{I}(k_x,k_y), \tag{A.7}$$

$$v_n(0) \equiv [v_n(t)]_{t=0} \equiv -\left[\frac{1}{\mathcal{K}c_\mathrm{s}^2}\frac{\mathrm{d}^2 v_{n-1}(t)}{\mathrm{d}t^2}\right]_{t=0}, \tag{A.8}$$

where

$$\mathcal{K} \equiv k_\mathrm{H}^2 + k_y^2 + k_x^2, \tag{A.9}$$

$$k_\mathrm{H}^2 \equiv \frac{4\Omega_0(\Omega_0 + A)}{c_\mathrm{s}^2}. \tag{A.10}$$

The principal concern with such a solution is its convergence. For instance, this solution diverges at $t = t^*$, when $k_x(t^*) = 0$ ($A \neq 0$). The area of the divergence strongly depends on the value of the shear rate. In our analysis we consider moderate shear rates, when $A/(k_y c_\mathrm{s}) \leq 1$. In this case the above series is convergent for times when $|k_x(t)/k_y| > 1$. Moreover, the first two term of this series appears to be an excellent approximation to the exact numerical solution for times when $|k_x(t)/k_y| \geq 2$. Therefore, we can use this analytic solution to compose the vortex mode perturbations that are localized in the wavenumber plane outside the $|k_x(t)/k_y| \leq 1$ area. We calculate the $v_y(k_x,k_y,0)$ and it's derivative for the vortex mode perturbations in explicit form:

$$v_y(k_x,k_y,0) = \left(\frac{k_x}{\mathcal{K}} + \frac{8A^2 k_x k_y^2}{c_\mathrm{s}^2}\cdot\frac{3k_H^2 + 3k_y^2 - k_x^2}{\mathcal{K}^4}\right)\mathcal{I}(k_x,k_y), \tag{A.11}$$

$$v_y'(k_x,k_y,0) = \left(2Ak_y\frac{k_x^2 - k_y^2 - k_H^2}{\mathcal{K}^2} - \frac{16A^3k_y^3}{c_\mathrm{s}^2} \times\frac{3k_H^4 + 6k_H^2k_y^2 - 24k_H^2k_x^2 + 3k_y^4 + 5k_x^4 - 24k_x^2k_y^2}{\mathcal{K}^5}\right) \times\mathcal{I}(k_x,k_y), \tag{A.12}$$

where

$$v_y'(k_x,k_y,0) = \left[\frac{\mathrm{d}}{\mathrm{d}t}v_y(k_x(t),k_y,t)\right]_{t=0}.$$

Remaining physical quantities may be defined using the following equations:

$$v_x(k_x,k_y,0) = \frac{1}{4(\Omega_0 + A)^2 + k_y^2 c_\mathrm{s}^2}\Big[k_x k_y c_\mathrm{s}^2 v_y(k_x,k_y,0) - 2(\Omega_0 + A)v_y'(k_x,k_y,0) + k_y c_\mathrm{s}^2 \mathcal{I}(k_x,k_y,)\Big],$$

$$\frac{p(k_x,k_y,0)}{c_\mathrm{s}^2} = \varrho(k_x,k_y,0) = \frac{\mathrm{i}\rho_0}{2(\Omega_0 + A)}\Big[k_x v_y(k_x,k_y,0) - k_y v_x(k_x,k_y,0) - \mathcal{I}(k_x,k_y)\Big]. \tag{A.13}$$

Hence, using any distribution of the potential vorticity $\mathcal{I}(k_x,k_y)$ (or $v_y(k_x,k_y,0)$) and Eqs. (A.9)−(A.14) we can construct corresponding initial vortex mode perturbation in the wavenumber plane.